Accepted for publication in Polymer Testing
Published in March 6, 2014
DOI: 10.1016/j.polymertesting.2014.03.003

Polymer testing

Thermal, viscoelastic and mechanical behaviors of polypropylene with synthetic boehmite alumina nanoparticles

D. Pedrazzoli [(a)], V. M. Khumalo[(b,c)],
J. Karger-Kocsis[(c,d,e)], A. Pegoretti [(a)]*

[(a)] Department of Industrial Engineering and INSTM Research Unit, University of Trento, Trento, 38123 (Italy)
[(b)] Polymers and Composites, Materials Science and Manufacturing, Council for Scientific and Industrial Research, CSIR, P.O. Box 395, Pretoria 0001 (South Africa)
[(c)] Polymer Technology, Faculty of Mechanical Engineering and Built Environment, Tshwane University of Technology, Pretoria 0001 (South Africa)
[(d)] MTA–BME Research Group for Composite Science and Technology, Muegyetem rkp. 3., H-1111 Budapest (Hungary)
[(e)] Polymer Engineering, Faculty of Mechanical Engineering, Budapest University of Technology and Economics, H-1111 Budapest (Hungary)

*Corresponding author.
Tel.: +39-0461-282452; fax: +39-0461-281977
e-mail address: a.pegoretti@ing.unitn.it (A. Pegoretti)

Abstract

Effects of nanofiller concentration and surface treatments on the morphology, thermal, viscoelastic and mechanical behaviors of polypropylene copolymer (PP)/boehmite alumina (BA) nanocomposites were investigated. Both untreated and treated BA particles with octylsilane (OS) and with sulphonic acid compound (OS2) were added up to 10 wt% to produce nanocomposites by melt mixing followed by film blow molding and hot pressing. Dispersion of BA was studied by scanning electron microscopy. Differential scanning calorimetry and wide-angle X-ray scattering were adopted to detect changes in the crystalline structure of PP. Thermooxidative degradation of the nanocomposites was assessed by thermogravimetrical analysis. Dynamic mechanical analysis served for studying the viscoelastic, whereas quasi-static tensile, creep and Elmendorf tear tests were used to detect changes in the mechanical performance. BA nanoparticles were finely dispersed in PP up to 10 wt%, even when they were not surface modified. The resistance to thermal degradation was markedly improved by BA nanomodification. Changes observed in the mechanical properties were attributed to BA dispersion, filler/matrix interactions and related effects because the crystalline characteristics of the PP matrix practically did not change with BA modification.

Keywords

Nanocomposite; Boehmite alumina; Morphology; Thermal properties; Mechanical properties; Tear resistance; Short term creep

1. Introduction

Increasing efforts are devoted to the research of thermoplastic nanocomposites exhibiting improved and novel properties. Most of these studies are focused on the investigation of correlations between structural features and mechanical properties [1-3]. In particular, considerable resources have been dedicated in the research of thermoplastic matrices modified with polar nanofillers (such as silicas, metal oxides, metal salts, layered silicates, etc…) in order to enhanced their thermal, mechanical and rheological performances [4-8]. On the other hand, these nanofillers are generally poorly dispersed in apolar thermoplastics (such as polyolefins), thus limiting their beneficial effects on the target thermo-mechanical properties. In order to enhance the dispersibility of nanofillers in polyolefins they are usually introduced after surface treatment [9-11] or together with suitable polymeric compatibilizers [12-16]. Nevertheless, with the aim of avoiding additional costs and processes, researchers have been looking for nanofillers which can be easily and homogeneously dispersed within the polymeric matrix without use of compatibilizers or surface treatments on the nanoparticles.

With this regards, synthetic boehmite alumina (BA), with chemical composition n-AlO(OH),represents an ideal candidate thanks to its inexpensive and easy production process [17-20]. Its primary particle size is in the range of tens of nanometers. BA has recently become the subject of research attention as a new type of additive for enhancing the mechanical, thermal and fire-retardant performances of polymers [21-25]. In order to get a deeper understanding on the structure-property relationships, two BA grades with different primary particle size were incorporated in both low density and high density polyethylenes (LDPE and HDPE, respectively) by melt compounding. It was found that BA was nanoscale dispersed within these matrices and did not influence the rheological properties of the corresponding PEs. On the other hand, BA dramatically enhanced the resistance to thermo-oxidative degradation of PEs [19]. Furthermore, it was found that BA worked as reinforcing filler according to quasi-static mechanical tests and dynamic mechanical thermal analysis (DMTA). Interestingly, the perforation impact resistance of PEs nanocomposites was reduced with increasing BA content, finding that the lesser the reduction the higher the primary particle size of the used BA was [20].

Polypropylene (PP) does not include any polar groups in its backbone that could interact with the BA [26], resulting in a limited dispersion level of the BA in the PP matrix and in poor interfacial adhesion between filler and matrix. This is usually accompanied with limited reinforcing effect. Nevertheless, the compatibilization strategies between fillers and PP include the addition of polymeric compatibilizers [12, 14-16] and the pre-treatment of fillers with coupling agents [27-31]. In particular, Özdilek et al. investigated the effects of both untreated and surface treated BA on the thermo-mechanical behavior and morphology of polyamide 6 (PA 6) nanocomposites, showing that the polymer crystalline structure is significantly changed and the storage modulus is doubled upon inclusion of BA particles [18, 23]. Ogunniran studied the

effect of the incorporation of BA in PP/PA 12 blends, finding that the degree of compatibility of the two polymers increased at high nanoparticle loading and BA significantly improved the thermal and mechanical properties [18, 32]. In a previous work of our group the influence of BA content and surface treatment was investigated with respect to the morphology, crystallization behavior and mechanical properties of PP copolymer nanocomposites [33]. Specifically, the effects of untreated and surface modified (with octylsilane and sulphonic acid compound, respectively) BA nanoparticles with a crystallite size of around 80 μm on the thermo-mechanical properties were investigated. The present work was aimed at studying how the addition of BA nanoparticles with crystallite size of 40 nm with and without surface functionalization affects the morphology, thermal and mechanical properties of PP copolymer nanocomposites. BA was incorporated up to 8 wt% in untreated, octylsilane (OS) and alkylbenzene sulphonic acid (OS2) modified forms, respectively. Beside of static tensile , the mechanical tests covered also the creep and tear resistance of the related nanocomposites which are rarely addressed.

2. Experimental section

2.1 Materials and samples preparation

As matrix polypropylene impact copolymer, namely CHR 440 type of Sasol (Sasolburg, South Africa), was selected. Its melt flow index measured at 230°C and 2.16 kg was 1.5 g/10 min and its density 0.905 $g \cdot cm^{-3}$. Synthetic boehmite Disperal®40, provided by Sasol GmbH (Hamburg, Germany), was used as nanofiller in pristine (BA40) and in surface treated forms. Surface functionalization occurred by octylsilane (BA40-OS) and by C10–C13 alkylbenzene sulphonic acid (BA40-OS2), respectively. The nominal primary crystallite size of the pristine form is 40 nm, while the specific surface area is 105 $m^2 \cdot g^{-1}$[19]. BA was incorporated into the PP in 2.5, 5 and 10 wt%, respectively.

Samples were prepared by melt mixing using a Berstorff co-rotating twin-screw extruder (ZE-40, Berstorff, Hannover, Germany) followed by granulation. The barrel temperatures from the hoper to die were 185, 185, 195, 195, 205, 205,220, 220°C, the screw rotated at 100 rpm and the melt passed through the extruder in ca. 80 s. The granules were successively blow molded (extruder-film blowing machine, 25 mm extruder type, model LE25-30/CV of Labtech Engineering, Bangkok, Thailand) in order to produce film sheets with thickness of around 0.6 mm. The barrel temperatures from the hopper to die were 180, 185, 190, 195, 200 °C, the screw rotated at 65 rpm and the pressure was 21 MPa. The die temperatures were 200, 210, 220 °C. The rolling speed of nip rollers and pulling rollers was 3.1 and 3.8 $m \cdot min^{-1}$, respectively, while the blower pressure was set to 0.4 MPa. The specimens used for DMTA were cut from the blow molded sheets along the machine

direction. On the other hand, the specimens necessary for the Elmendorf tear test were obtained along both machine and transverse direction.

Bulk specimens, necessary for the quasi-static tensile tests, were produced by compression molding of the granules using a P.H.I hydraulic press (Pasadena Hydraulics Inc, La Puente, CA, USA) in order to produce square sheets with thickness of 4.2 mm. The material was heated to 190°C while applying a pressure of 25 MPa for 15 min and then cooled to room temperature by water flow. The unfilled matrix was denoted as PP, while the code of the nanocomposites indicated the matrix, the filler weight amount and filler type. For instance, a sample filled with 5 wt% octylsilane treated BA is indicated as PP/5BA40-OS.

2.2 Experimental

2.2.1 Spectroscopy analysis

Dispersion of the BA nanoparticles was inspected on the cryo-fractured surfaces of the nanocomposites in scanning electron microscope (SEM; JEOL JSM-6380LA, Tokyo, Japan). Their electric conductivity was guaranteed by coating with an Au/Pd alloy.

2.2.2 Diffraction analysis

Wide angle X-Ray scattering (WAXS) spectra were taken by a Phillips® (PANalytical, Almelo, The Netherlands) diffractometer, using CuK_{α} irradiation (0.154056 nm). Typical scans were performed within a 2θ range between 5° and 40° and sampling interval of 0.02°.

2.2.3 Thermal analyses

Differential scanning calorimetry (DSC) was carried out by a Q2000 (TA Instruments® , New Castle, USA) differential scanning calorimeter under a constant nitrogen flow of 25 ml·min^{-1}. Samples were heated up to 200 °C at a rate of 10 °C·min^{-1} and cooled to 0 °C at a cooling rate of 10 °C·min^{-1}. A second heating scan was then performed at 10 °C·min^{-1}. Each melting scan was characterized by two temperatures, namely peak maximum ($T_{m,max}$) and final melting ($T_{m,final}$), and the crystallinity value (χ_m).The latter was estimated by taking the weight fraction of PP in the composites into account and accepting that the melting enthalpy of the 100% crystalline isotactic PP is equal to ΔH^0= 209 J·g^{-1}[34]. Also the crystallization behavior was characterized by two temperatures, namely peak maximum ($T_{c,max}$) and the initial temperature

of crystallization ($T_{c,initial}$). The crystallinity value (χ_c), received upon cooling, was determined as the ratio of crystallization enthalpy (ΔH_c) with respect to ΔH^0.

Thermogravimetric analysis (TGA) traces were registered on a Q5000 IR thermogravimetric analyzer (TA Instruments-Waters LLC, New Castle, USA) imposing a temperature ramp between 40 and 700 °C at a heating rate of 10 °C·min^{-1} under a constant nitrogen flow of 25 ml·min^{-1}.The thermal degradation behavior was quantified on TGA traces by the temperature associated with a weight loss of 2 and 10%, $T_{2wt\% loss}$ and $T_{10wt\% loss}$, respectively, and the residue value.

2.2.4 Mechanical tests

2.2.4.1 Quasi-static tensile tests

Uniaxial quasi-static tensile tests were performed at room temperature using an Instron® 5966 (Norwood, USA) tensile machine on samples of at least five specimens with cross section of 10 x 4.1 mm^2 and adopting a distance between grips of 85 mm. The tests were carried out at a crosshead speed of 50 mm·min^{-1}. In accordance to ISO 527 standard, the elastic modulus was measured as a secant value between deformation levels of 0.05 % and 0.25 %. Uniaxial tensile properties, such as stress at yield (σ_y) and strain at break (ε_b) were also determined.

2.2.4.2 Dynamic mechanical thermal analysis (DMTA)

DMTA tests were carried out in tensile mode with a DMA Q8000 testing machine (TA Instruments®, New Castle, USA) on rectangular specimens 25 mm long, 8 mm wide and 0.6 mm thick. The samples were analyzed over a temperature range between -50 °C and 180 °C, imposing a heating rate of 3 °C·min^{-1}in nitrogen atmosphere and setting a frequency of 1 and 10 Hz. The amplitude of the dynamic deformation of 1 μm was set for each test. The most important viscoelastic functions (*E', E'', tan(δ)*) were recorded at different temperatures. By the same apparatus, short term (3600 s) tensile creep tests at 30 °C were also performed at a constant applied stress (σ_0) of 4 MPa. The latter value was at 10% of the stress at yield of the unfilled PP.

2.2.4.3 Elmendorf-type tear tests

Propagation tear tests were performed using an Elmendorf-type tearing tester ED30 (Ceast®, Torino, Italy) on film specimens (thickness of about 0.6 mm) following the standard ASTM D1922. The tests were carried out on at least five specimens cut from the blow molded film along the machine and transverse directions, respectively. The propagation tear resistance was measured as the ratio of force (mN) required to propagate tearing across the specimen with respect to the

specimen thickness (μm). The force reading was corrected by a multiplication factor of 0.10197 in order to be converted in $g \cdot \mu m^{-1}$.

3. Results and discussion

3.1 Morphology

SEM pictures taken from the cryo-fractured surface of PP containing the same amount (5 wt%) of BA40 and BA40-OS nanoparticles are given in Fig. 1(a-b). BA particles appear quite well dispersed in the PP nanocomposite filled with untreated BA particles, although some agglomerates with average sizes of 300– 400 nm are recognizable. The compounding process seems to be effective even in the case of untreated particles, resulting in a good deagglomeration and rather uniform dispersion of the BA nanoparticles. Furthermore, some cavities and humps in micronscale are observable on the fracture surface which can be attributed to the rubber (i.e. ethylene-propylene) phase of the PP copolymer (Fig. 1a). On the other hand, the filler dispersion within the polymer matrix is only slightly improved by surface functionalization with silane coupling agent. In fact, the BA nanofiller appears organized in smaller and more uniformly distributed BA aggregates in the matrix (Fig. 1b).

BA nanoparticles remain finely dispersed also when added in higher amounts. In fact, Fig. 1c reveals good submicrometer size filler dispersion for the PP containing 10 wt% of BA40-OS nanoparticles. The SEM pictures substantiate that BA nanoparticles can be finely dispersed in PP up to 10 wt%, even when no surface functionalization is applied on the filler or polymeric compatibilizer is added to the matrix.

WAXS patterns of BA nanopowders showed that no crystallinity change occurred due to surface treatment applied (Fig. 2a). Moreover, WAXS performed on PP nanocomposites indicated no significant variation in the crystalline structure of PP owing to incorporation of BA with and without surface treatments (Fig. 2b). This is in line with the crystallinity values derived from DSC scans, as will be shown later (cf. Table 1).

3.2 Thermal properties

Since the matrix crystallinity may have an influence on the mechanical properties of nanocomposites, DSC experiments were carried out in order to investigate the crystallization and melting behavior of PP/BA nanocomposites. Incorporation of the filler produces a moderate increase of the crystallization peak temperature for all kinds of BAs, but no particular dependence of the nucleating effect as a function of the BA types is evidenced (Table 1). Interestingly, the crystallization peak temperature only slightly increases with the addition of BA40-OS2, when compared to composites containing BA40

and BA40-OS.This may be probably due to increased interaction between matrix and BA40-OS2 nanoparticles, which may retard the migration of the PP chains onto the growing crystal nucleus.

The weak nucleation effect of BA is observable more clearly when $T_{c,initial}$ instead of $T_{c,max}$ values are considered. While the data obtained from the first scan might suggest that BA increased the crystallinity of PP in the corresponding nanocomposites, the results from the second heating do not confirm this effect. Note that the latter data are more relevant as they reflect samples with the same thermal history. The melting behavior was practically not affected by BA incorporation.

The thermal resistance parameters, as detected in TGA measurements, are reported in Table 2. Both $T_{2wt\% loss}$ and $T_{10wt\% loss}$ noticeably increase with the filler content in all PP/BA40 nanocomposites, showing a slightly higher efficiency in PP/BA40-OS2 samples. This effect could also be linked with the dehydration process of BA nanofiller which delays the polymer degradation. Indeed, TGA analyses conducted on the fillers BA40 and BA40-OS alone show a comparable residue value slightly above 80%, probably indicating the loss of crystal water. On the other hand, the residue value recorded for the filler BA40-OS2 appears relatively lower (i.e. 63.7%), likely due to the loss of part of the organic surface treatment.

Representative TGA traces are depicted in Fig. 3 for PP and PP/BA40 nanocomposites. Improved thermal and thermo-oxidative stability due to the addition of BA has been already reported for PEs [19], PP [35, 36] and linear low density polyethylene [37]. It was recently demonstrated on LDPE/BA nanocomposites that the improved resistance of the thermo-oxidative stability due to BA filling is exclusively of physical origin and linked with the barrier effect of the nanoparticles hampering the diffusion of the gaseous degradation products [38].

3.3 Tensile mechanical behavior

The addition of BA40 nanoparticles increases the elastic modulus of the PP matrix, reaching an improvement of 15 % for systems filled with 10 wt% of nanofiller, compared to unfilled PP (Table 3). The stiffening effect induced by nanofiller incorporation is usually attributed to the formation of a rigid interphase between the matrix and the particles. Nevertheless, it has also been recently proposed that nanoparticles aggregation can be another mechanism responsible for stiffness increase in polymer nanocomposites [38, 39]. When the properties at yield and at break of the PP/BA40 composites are considered with respect to the unfilled matrix, it can be observed that the yield strength slightly increases, while the elongation at break is also enhanced, reaching a maximum for the filler content of 2.5 wt%. A similar behavior was reported by Khumalo et al. for the tensile yield and elongation at break of HDPE/BA nanocomposites [20]. In particular, the enhanced ductility can be explained by a failure mode in which particle debonding with massive voiding occurs first, followed by void coalescence associated with matrix fibrillation [20].

The addition of BA40-OS nanoparticles results in a remarkable enhancement of the material ductility, producing an increase in strain at break of 163% for the system PP/5BA40-OS, while elastic modulus and yield strength only slightly increase. The increased ductility shown in PP/BA40-OS composite can be attributed to either a reduction in the molecular weight of PP by the octylsilane compound the improved adhesion between PP and BA40–OS, or both processes took place. A significant reduction in the molecular weight should be associated to a crystallinity increase, but, this not the case (Table 1). Nanocomposites with BA40-OS2 show the highest enhancement in yield strength with respect to the other systems. On the other hand, nanofiller addition produces a noticeable decrease in strain at break, probably because of strong interaction between filler and matrix [12]. Although an increase was expected as a result of smaller agglomerations, the opposite happened. It seems that, the sulphonic acid surface treatment of BA promotes a greater interaction between matrix and particles. As a result, the BA nanoparticles do not participate in massive debonding followed by fibrillation which inhibits the macroscopic elongation of the corresponding nanocomposite [33].

3.4 Viscoelastic behavior

The dynamic-mechanical response of PP is markedly affected by the addition of BA40 nanoparticles. In particular, the storage modulus (*E'*) increases remarkably as the BA40 content increases, probably due to the restrictions of the molecular chains motion (Table 4). Accordingly, the material's stiffness and load bearing capability increase. The addition of BA40 produces the highest enhancement in *E'*, when compared to the other nanocomposites. Nanofiller incorporation also results in a significant increase of the loss modulus (*E''*). The glass transition temperature (T_g), evaluated in correspondence of the *tan (δ)* peak, was slightly higher for PP/BA40 nanocomposites with respect to unfilled PP, indicating the restriction of the motion of polymer chains induced by the nanofillers incorporation. As expected, DMTA measurements conducted at a frequency of 10 Hz show higher values in moduli but slightly lower T_g and *tan (δ)* peak values.

The stiffness of PP/BA40-OS nanocomposites was lower than the reference PP in the whole temperature range studied, in accordance to results of quasi-static tensile tests. Interestingly, incorporation of BA40-OS particles resulted in a slight increase in the T_g, probably indicating an effective interfacial interaction between the BA nanoparticles and the PP matrix [9]. Incorporation of PP/BA40-OS2 particles results in a remarkable increase in stiffness at a content of 2.5 wt%, while a progressive decrease occurs at higher filler amounts. These results are in good agreement with the modulus trend observed in quasi-static tensile tests. Comparison plots of the storage modulus (*E'*) and loss factor (*tan δ*) evaluated at 1 Hz are displayed in Fig. 4a and Fig. 4b, respectively, as a function of temperature for unfilled PP and its nanocomposites containing 10 wt% BA.

In Fig. 5 the isothermal creep compliance of PP and PP/10BA40 nanocomposites, under a constant load of 4 MPa and at 30 °C, is reported, while in Table 4 the total creep compliance after 3600 s ($D_{tot,3600s}$) is reported. The introduction of BA nanoparticles results in a significant improvement of the creep stability of the material in the case of PP/BA40. It is generally believed that nanoparticles can effectively restrict the motion of polymer chains, influencing the stress transfer at a nanoscale, with positive effects on the creep stability of the material [40]. On the other hand, the addition of BA40-OS nanoparticles leads to lower creep compliance with respect to unfilled PP only at filler contents as high as 10 wt%. Moreover, incorporation of BA40-OS2 filler results in a slightly higher creep compliance when compared to unfilled PP. Since the creep compliance can be factorized into the elastic and visco-elastic components, creep results are generally in good agreement with the modulus trend observed in quasi-static tensile tests

3.5Propagation tear resistance

Due to orientation during their manufacture, plastic films and sheeting frequently show marked anisotropy in their resistance to tearing. This is further complicated by the fact that some films elongate greatly during tearing. The degree of this elongation is dependent on film orientation and the inherent mechanical properties of the polymer from which it is made [41].The Elmendorf tearing energy (Fig. 6) of the PP nanocomposites decreased with the BA content for PP/BA40 and PP/BA40-OS2 samples, whereas it was noticeably increased at low BA contents and gradually decreased for higher filler loadings in PP/BA40-OS composites. Moreover, a marked anisotropy is observable in PP nanocomposites with respect to unfilled PP (Table 3).This effect could happen because of variations in molecular weight distribution due to nanomodification, which produces a change in molecular orientation and in turn affects many physical properties included tear strength[42]. However, as already seen in the case of tensile properties, this is not the case. A more probable reason is represented by a higher macro orientation occurring in nanocomposites during manufacturing. Nevertheless, in order to obtain a deeper understanding of this phenomenon, rheology measurements would be required.

Noteworthy, results of tear resistance are in good agreement with values of strain at break obtained in tensile tests.

The microvoids formation might be responsible for the increment in toughness in PP/BA40-OS samples. As already observed by Soundararajan in the case of poly(vinyl alcohol) nanomodified with montmorillonite, these microvoids release the plastic constraint in the matrix, triggering large-scale plastic deformation with consequent tearing of matrix ligaments between microvoids. Moreover, the higher the filler content, the larger the aggregates and agglomerates, resulting in brittle fracture and limiting the microvoid formation. On the other hand, only crazing contributes to energy absorption in neat PP, which is much lower in comparison [43].

Interestingly, the incorporation of BA40-OS2 particles results in a prominent decrease in tear resistance, probably due to the greater interaction established between matrix and particles which strongly inhibits the deformation and tearing capabilities of the nanocomposite. Unfortunately, no tear results were available for the PP/5BA40-OS2 and PP/10BA40-OS2 samples, as the formation of a great amount of bubbles during the film processing strongly limited the possibility of obtaining wide enough specimens for tear testing.

4. Conclusions

In this study, effects of boehmite nanoparticles (BA) with different surface treatments on the morphology, thermal, viscoelastic and mechanical behaviors of a PP copolymer were investigated. PP/BA nanocomposites containing 2.5, 5 and 10 wt % BA with and without surface treatments were prepared. The BA particles were treated with octylsilane (OS) and with sulphonic acid compound (OS2).The incorporation of surface treated nanoparticles resulted in a slightly better dispersion of the filler within the matrix, as confirmed by SEM observations.

BA acted as a weak nucleation agent in PP matrix, producing slight increases in crystallinity and in the crystallization temperature. By contrast, a substantial enhancement of the degradation properties took place thanks to the nanomodification.

The increased tensile modulus recorded in PP/BA composites was associated with a slight enhancement of the elongation at break. PP/BA-OS systems showed a remarkable increase in ductility upon filler introduction, whereas the incorporation of BA-OS2 particles yielded a less ductile material. This was explained by differences in the filler/matrix interactions governing the failure sequence and mode. The observations regarding tensile tests were in line with the changes observed for the storage and loss modulus in DMTA tests and creep resistance. The propagation tear resistance increased at low filler contents in the case PP/BA-OS composites. In this case, the nucleation of microvoids had a positive effect in the enhancement of tearing energy while the agglomeration of BA particles had a negative effect.

Acknowledgement

This work was performed in the framework of a bilateral cooperation agreement between Italy (HU11MO8) and Hungary (TÉT_10-1-2011-0218).

References

[1] F Tuba, VM Khumalo, J Karger-Kocsis (2013) Journal of Applied Polymer Science. Doi:10.1002/APP.39004
[2] W Brostow, T Datashvili, B Huang, J Too (2009) Polymer Composites 30: 760. Doi:10.1002/pc.20610
[3] K-S Lee, Y-W Chang (2012) Journal of Applied Polymer Science: 1. Doi:10.1002/app.38457 10.1002/APP.38457
[4] A Durmus, A Kasgöz, C Macosko (2008) Journal of Macromolecular Science, Part B 47: 608. Doi:10.1080/00222340801957780
[5] A Durmus, A Kasgoz, CW Macosko (2007) Polymer 48: 4492. Doi:10.1016/j.polymer.2007.05.074
[6] S Hotta, DR Paul (2004) Polymer 45: 7639. Doi:10.1016/j.polymer.2004.08.059
[7] A Dorigato, A Pegoretti, A Frache (2012) Journal of Thermal Analysis and Calorimetry 109: 863. Doi:10.1007/s10973-012-2421-4
[8] P Kiliaris, CD Papaspyrides (2010) Progress in Polymer Science 35: 902. Doi:10.1016/j.progpolymsci.2010.03.001
[9] MZ Rong, MQ Zhang, SL Pan, B Lehmann, K Friedrich (2004) Polymer International 53: 176. Doi:10.1002/pi.1307
[10] H Zou, S Wu, J Shen (2008) Chemical Reviews 108: 3893. Doi:10.1021/cr068035q
[11] R-J Zhou, T Burkhart (2010) Journal of Materials Science 46: 1228. Doi:10.1007/s10853-010-4901-x
[12] DN Bikiaris, A Vassiliou, E Pavlidou, GP Karayannidis (2005) European Polymer Journal 41: 1965. Doi:10.1016/j.eurpolymj.2005.03.008
[13] O Lin, Z Mohd Ishak, H Akil (2009) Materials & Design 30: 748. Doi:10.1016/j.matdes.2008.05.007
[14] S-P Liu, J-R Ying, X-P Zhou, X-L Xie, Y-W Mai (2009) Composites Science and Technology 69: 1873. Doi:10.1016/j.compscitech.2009.04.004
[15] H Mirzazadeh, AA Katbab, AN Hrymak (2011) Polymers for Advanced Technologies 22: 863. Doi:10.1002/pat.1589
[16] B Mohebby, P Fallah-Moghadam, AR Ghotbifar, S Kazemi-Najafi (2011) Journal of Agricolture Science and Technology.
[17] P Blaszczak, W Brostow, T Datashvili, HEH Lobland (2010) Polymer Composites 31: 1909. Doi:10.1002/pc.20987
[18] C Özdilek, K Kazimierczak, SJ Picken (2005) Polymer 46: 6025. Doi:10.1016/j.polymer.2005.05.065
[19] VM Khumalo, J Karger-Kocsis, R Thomann (2010) eXPRESS Polymer Letters 4: 264. Doi:10.3144/expresspolymlett.2010.34
[20] VM Khumalo, J Karger-Kocsis, R Thomann (2010) Journal of Materials Science 46: 422. Doi:10.1007/s10853-010-4882-9
[21] CY Chee, NL Song, LC Abdullah, TSY Choong, A Ibrahim, TR Chantara (2012) Journal of Nanomaterials 2012: 1. Doi:10.1155/2012/215978
[22] ES Ogunniran, R Sadiku, S Sinha Ray, N Luruli (2012) Macromolecular Materials and Engineering 297: 237. Doi:10.1002/mame.201100148
[23] C Özdilek, B Norder, SJ Picken (2008) Thermochimica Acta 472: 31. Doi:10.1016/j.tca.2008.03.008
[24] J Zhang, Q Ji, P Zhang, Y Xia, Q Kong (2010) Polymer Degradation and Stability 95: 1211. Doi:10.1016/j.polymdegradstab.2010.04.001
[25] K Das, S Sinha Ray, S Chapple, J Wesley-Smith (2013) Industrial & Engineering Chemistry Research 52: 6083. Doi:10.1021/ie4004305
[26] X Liu, Q Wu (2001) Polymer 42: 10013.
[27] K Prashantha (2011) Express Polymer Letters 5: 295. Doi:10.3144/expresspolymlett.2011.30
[28] A Askeland, Hiroyuki Fukushima, Inhwan Do, K Kalaitzidou, LT Drzal (2006) NSTI-Nanotech 2006,
[29] A Fina, HCL Abbenhuis, D Tabuani, A Frache, G Camino (2006) Polymer Degradation and Stability 91: 1064. Doi:10.1016/j.polymdegradstab.2005.07.013
[30] T Kuila, S Bose, AK Mishra, P Khanra, NH Kim, JH Lee (2012) Progress in Materials Science 57: 1061. Doi:10.1016/j.pmatsci.2012.03.002
[31] P Steurer, R Wissert, R Thomann, R Mülhaupt (2009) Macromolecular Rapid Communications 30: 316. Doi:10.1002/marc.200800754
[32] ES Ogunniran, R Sadiku, S Sinha Ray, N Luruli (2012) Macromolecular Materials and Engineering 297: 627. Doi:10.1002/mame.201100254
[33] D Pedrazzoli, F Tuba, VM Khumalo, A Pegoretti, J Karger-Kocsis (2013) Composites Part A Under submission.
[34] E James (1999) Polymer data handbook. Oxford University Press, New York
[35] RC Streller, R Thomann, O Torno, R Mülhaupt (2008) Macromolecular Materials and Engineering 293: 218. Doi:10.1002/mame.200700354

[36] S Bocchini, S Morlat-Thérias, J-L Gardette, G Camino (2007) Polymer Degradation and Stability 92: 1847. Doi:10.1016/j.polymdegradstab.2007.07.002
[37] D Pedrazzoli, R Ceccato, J Karger-Kocsis, A Pegoretti (2013) Express Polymer Letters 7: 652. Doi:10.3144/expresspolymlett.2013.62
[38] A Dorigato, Y Dzenis, A Pegoretti (2011) Procedia Engineering 10: 894. Doi:10.1016/j.proeng.2011.04.147
[39] A Dorigato, Y Dzenis, A Pegoretti (in press) Mechanics of Materials.
[40] F Bondioli, A Dorigato, P Fabbri, M Messori, A Pegoretti (2009) Journal of Applied Polymer Science 112: 1045. Doi:10.1002/app.29472
[41] A D1922-09 (2009),
[42] AJ Peacock, A Calhoun (2006) Polymer chemistry: properties and applications. Munich
[43] QY Soundararajah, BSB Karunaratne, RMG Rajapakse (2009) Journal of Composite Materials 44: 303. Doi:10.1177/0021998309347040

Figure captions

Fig. 1 SEM images of the cryo-fractured surfaces of (a) PP/5BA40, (b) PP/5BA40-OS and (c) PP/10BA40-OS nanocomposites.

Fig. 2 Wide-angle X-ray diffractograms of (a) BA40 nanopowders and (b) PP nanocomposites filled with 2.5 and 10 wt% BA versions. The curves were shifted vertically.

Fig. 3 Remaining mass as a function of temperature during TGA analysis performed on PP and PP/BA40 nanocomposites with different filler contents.

Fig.4 Dynamic mechanical properties of PP and its nanocomposites (f = 1 Hz): (a) Storage modulus (*E'*) and (b) Loss tangent (*tg(δ)*) as a function of temperature.

Fig.5 Creep compliance (D(t)) of PP and PP/BA40 nanocomposites (T=30 °C, σ_0 = 4 MPa).

Fig.6 Propagation tear resistance of PP nanocomposites as a function of the filler content along the machine (open symbol) and transverse (full symbol) direction.

Table 1. Melting and crystallization characteristics of PP and relative nanocomposites from DSC measurements

Sample	First melting			Crystallization			Second melting		
	$T_{m,max}$ [°C]	$T_{m,final}$ [°C]	χ_m [%]	$T_{c,max}$ [°C]	$T_{c,initial}$ [°C]	χ_c [%]	$T_{m,max}$ [°C]	$T_{m,final}$ [°C]	χ_m [%]
PP	166.7	174.6	35.2	122.2	129.8	37.8	167.3	174.8	38.2
PP/2.5BA40	166.6	173.8	37.1	123.0	130.2	38.6	168.3	175.6	38.8
PP/5BA40	166.6	173.9	36.9	124.1	131.0	39.4	166.9	174.4	40.1
PP/10BA40	166.1	173.8	38.3	129.8	135.6	40.6	167.6	174.0	40.3
PP/2.5BA40-OS	166.1	172.7	36.8	123.9	130.0	38.8	167.0	173.6	39.2
PP/5BA40-OS	165.5	173.1	39.5	124.3	130.1	39.2	166.5	173.3	39.4
PP/10BA40-OS	166.9	174.6	40.2	127.5	133.1	39.6	167.9	174.8	39.5
PP/2.5BA40-OS2	167.9	177.2	37.4	122.3	130.1	38.4	168.1	177.3	38.6
PP/5BA40-OS2	167.5	176.1	40.9	122.7	130.2	39.2	167.6	176.4	39.0
PP/10BA40-OS2	167.9	177.8	39.6	123.0	130.5	39.6	168.4	177.8	39.3

Table 2. TGA parameters on PP and relative nanocomposites.

Sample	$T_{2wt\% loss}$ [°C]	$T_{10wt\% loss}$ [°C]	Residue [%]
PP	382.6	430.0	0.3
PP/2.5BA40	383.5	431.7	2.9
PP/5BA40	388.7	437.2	4.4
PP/10BA40	393.4	442.6	9.5
PP/2.5BA40-OS	384.6	432.8	2.7
PP/5BA40-OS	388.5	437.6	4.6
PP/10BA40-OS	395.1	445.7	9.8
PP/2.5BA40-OS2	383.6	431.9	2.8
PP/5BA40-OS2	388.1	438.0	4.3
PP/10BA40-OS2	394.0	443.2	9.9
BA40 (*)	/	/	81.3
BA40-OS (*)	/	/	83.5
BA40-OS2 (*)	/	/	63.7

$T_{2wt\% loss}$:Temperature associated with a weight loss of 2 %.
$T_{10wt\% loss}$: Temperature associated with a weight loss of 10 %.
(*) Sample in form of nanopowder.

Table 3. Quasi-static tensile mechanical properties and propagation tear resistance of PP nanocomposites.

Sample	Tensile modulus [MPa]	Tensile Strength at Yield [MPa]	Elongation at Break [%]	Tear [g/μm] M.D.(*)	Tear [g/μm] T.D. (**)
PP	901 ± 9	28.5 ± 0.4	127±11	21.5 ± 0.9	24.1 ± 0.8
PP/2.5BA40	987 ± 15	30.2 ± 0.2	168 ± 18	16.5 ± 0.5	27.6 ± 3.5
PP/5BA40	1020 ± 32	30.4 ± 0.5	153 ± 18	15.8 ± 0.7	17.6 ± 0.4
PP/10BA40	1034 ± 25	30.2 ± 0.2	149 ± 28	10.0 ± 1.0	15.2 ± 1.4
PP/2.5BA40-OS	962 ± 34	28.9 ± 0.4	253 ± 103	22.5 ± 1.1	42.9 ± 2.0
PP/5BA40-OS	930 ± 5	29.0 ± 0.2	334 ± 87	14.6 ± 0.8	45.9 ± 6.0
PP/10BA40-OS	(***)	(***)	(***)	14.3 ± 0.9	34.0 ± 10.2
PP/2.5BA40-OS2	920 ± 18	31.4 ± 0.5	136 ± 26	11.0 ± 1.5	12.9 ± 2.0
PP/5BA40-OS2	933 ± 19	30.8 ± 0.6	116 ± 13	/	/
PP/10BA40-OS2	919 ± 3	29.6 ± 0.3	105 ± 41	/	/

(*) Machine direction.
(**) Transverse direction.
(***) No possibility of obtaining specimens for tensilemechanical testing

Table 4. Creep compliance data and dynamic mechanical properties of PP and relative nanocomposites evaluated at 1 Hz (upper value) and 10 Hz (lower value).

Sample	E' (-50 °C) [MPa]	E' (+23 °C) [MPa]	E'' (+23 °C) [MPa]	$T_{\beta peak}$[°C]	$tg(\delta)_{\beta peak} \cdot 10^{-2}$	$D_{tot,3600s}$ [GPa^{-1}]
PP	5160	2316	151	8.8	6.7	2.04
	5250	2300	147	8.4	7.1	
PP/2.5BA40	5030	1980	122	9.3	6.6	1.79
	5310	2260	124	8.4	6.4	
PP/5BA40	5380	2110	128	10.8	6.8	1.65
	5520	2240	132	8.5	6.5	
PP/10BA40	6830	3020	173	11.9	7.1	1.57
	6930	2870	174	9.3	7.0	
PP/2.5BA40-OS	4110	1990	135	8.4	7.0	1.89
	4500	2110	131	8.2	7.0	
PP/5BA40-OS	3670	1630	122	9.2	8.5	2.14
	3890	1720	124	9.1	8.5	
PP/10BA40-OS	4790	1960	112	9.5	6.4	1.64
	5060	2070	111	9.4	6.3	
PP/2.5BA40-OS2	5510	2210	161	7.4	6.9	2.10
	5720	2440	163	7.9	6.5	
PP/5BA40-OS2	5300	1860	155	9.9	9.6	/(*)
	5530	2000	163	9.6	9.3	
PP/10BA40-OS2	3720	1450	131	10.0	10.8	/(*)
	3910	1560	134	9.7	10.0	

E' (-50 °C) : storage modulus at -50 °C.
E' (+23 °C) : storage modulus at +23 °C.
E'' (+23 °C) : loss modulus at +23 °C.
$T_{\beta\ peak}$: temperature of β peak recorded in tg(δ) plots.
$tg(\delta)_{\beta peak}$: value of loss factor recorded in correspondence of β peak.
$D_{tot,\ 3600s}$: creep compliance recorded at 3600 s.

(*) No possibility of obtaining specimens for mechanical testing due to problems os bubble formation encountered during the production process.

Fig. 1

(a)

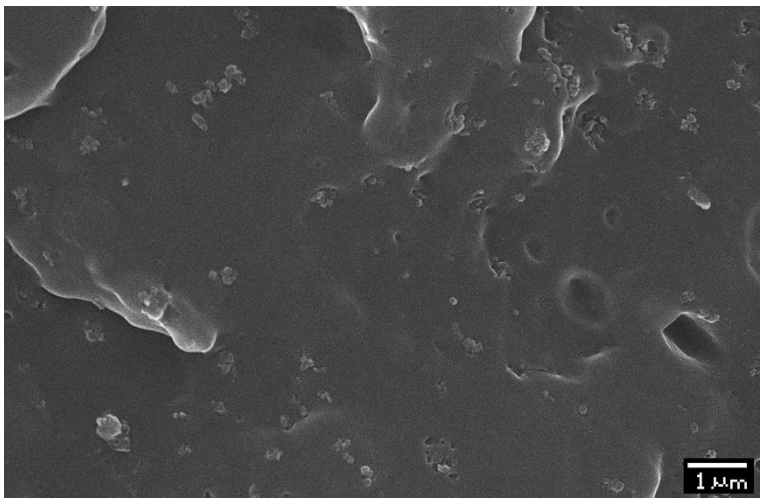

(b)

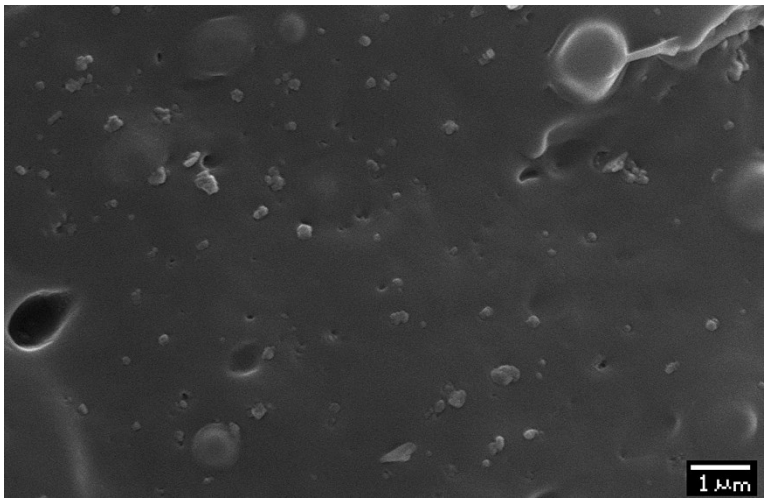

(c)

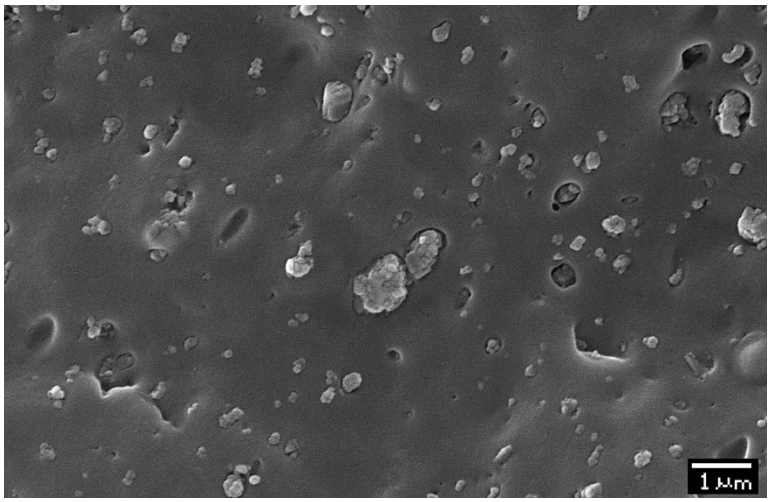

Fig. 2

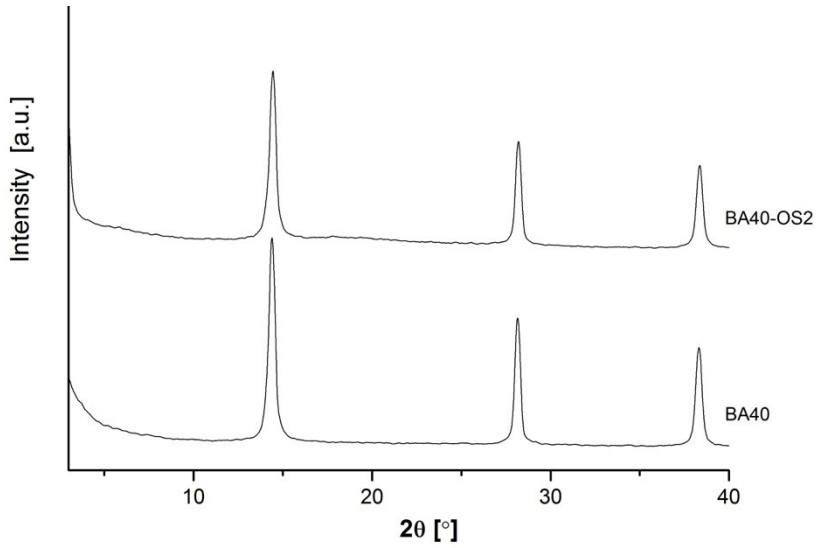
Intensity [a.u.]
BA40-OS2
BA40
10
20
30
40
2θ [°]

(a)

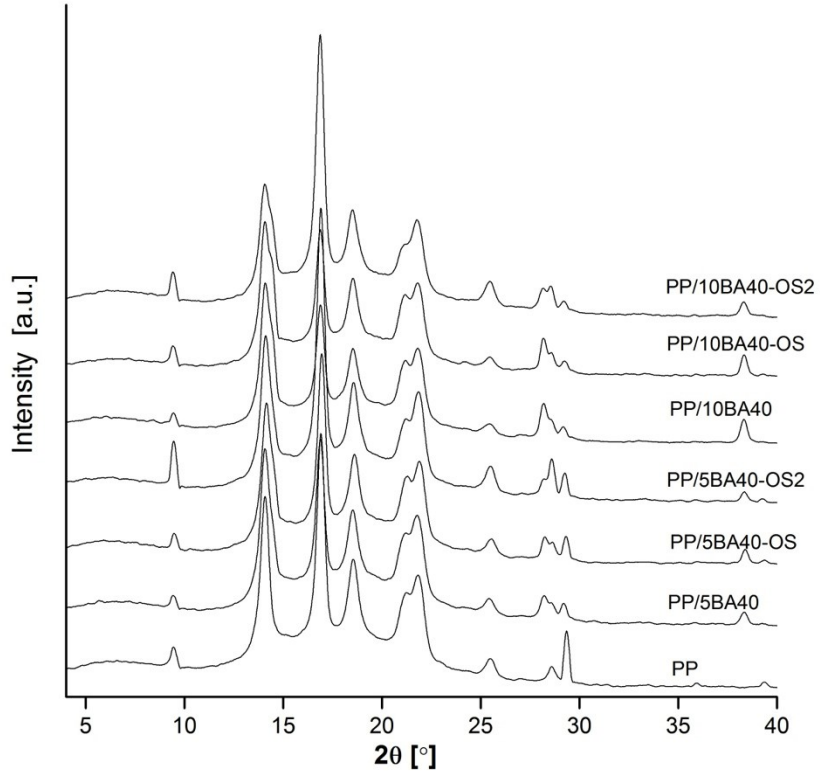
Intensity [a.u.]
PP/10BA40-OS2
PP/10BA40-OS
PP/10BA40
PP/5BA40-OS2
PP/5BA40-OS
PP/5BA40
PP
5
10
15
20
25
30
35
40
2θ [°]

(b)

Fig. 3

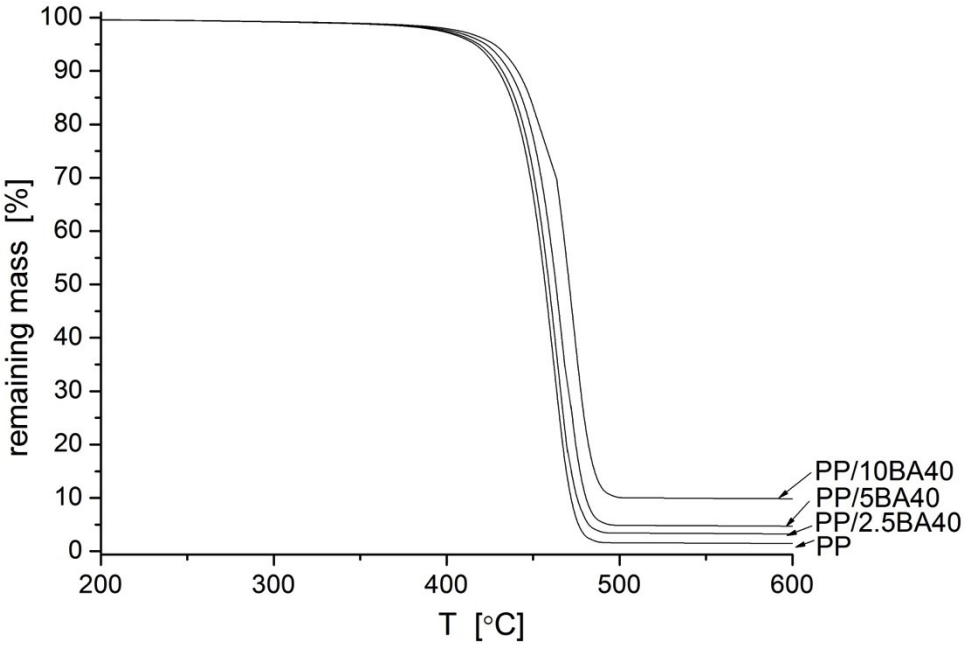

Fig. 4

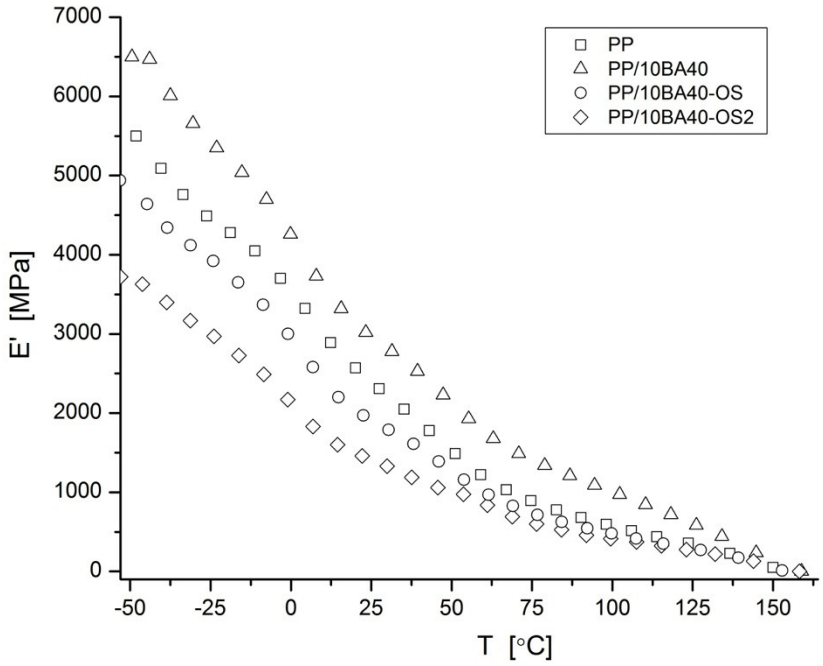
PP
PP/10BA40
PP/10BA40-OS
PP/10BA40-OS2
E' [MPa]
T [°C]

(a)

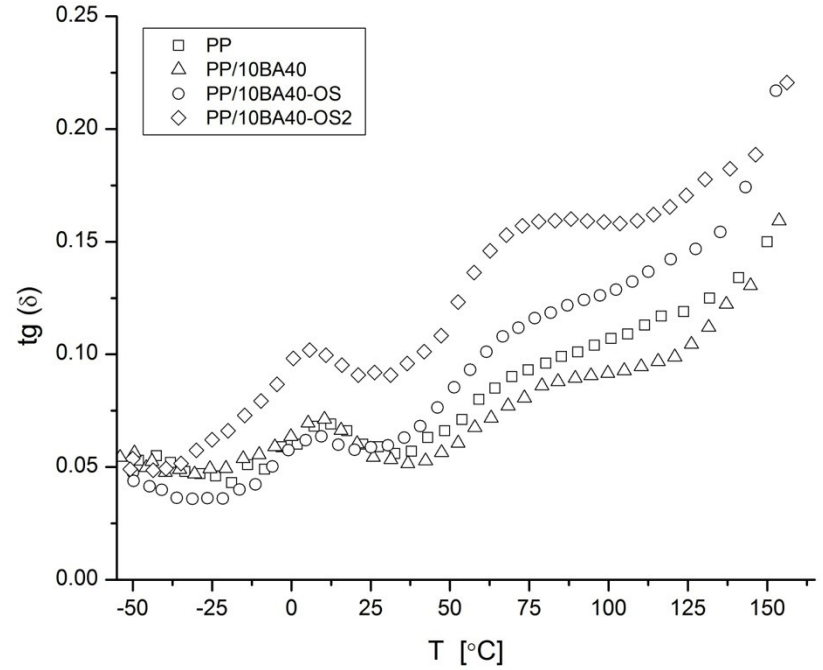
PP
PP/10BA40
PP/10BA40-OS
PP/10BA40-OS2
tg (δ)
T [°C]

(b)

Fig. 5

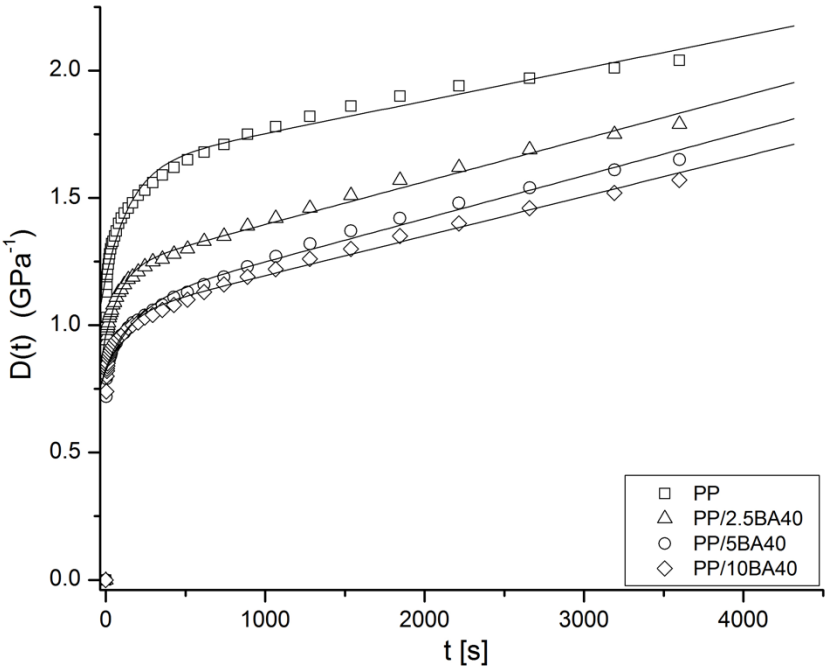
D(t) (GPa^{-1})
t [s]
PP
PP/2.5BA40
PP/5BA40
PP/10BA40

Fig. 6

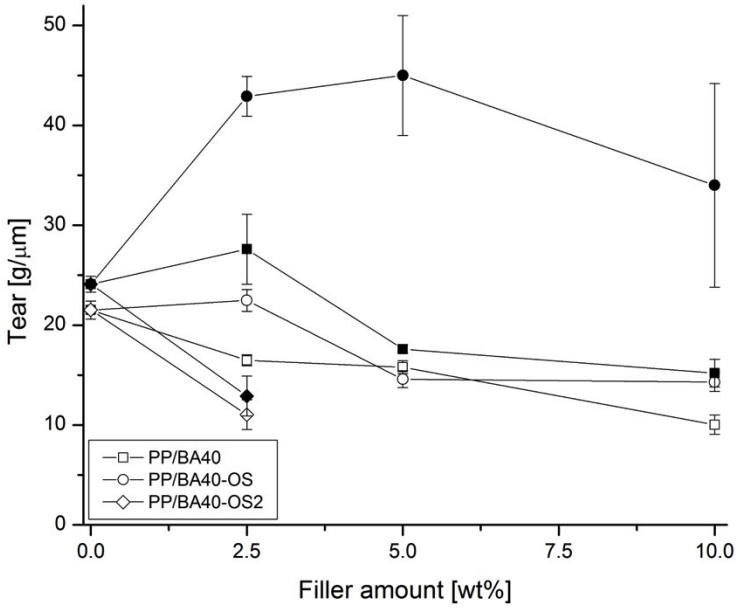
Tear [g/μm]
Filler amount [wt%]
PP/BA40
PP/BA40-OS
PP/BA40-OS2